

SUPPLEMENTARY MATERIAL

for

Luminescent Dual Sensors Reveal Extracellular pH-Gradients and Hypoxia on Chronic Wounds That Disrupt Epidermal Repair

Stephan Schreml, Robert J. Meier, Michael Kirschbaum,
Su Chii Kong, Sebastian Gehmert, Oliver Felthaus,
Sarah K uchler, Justin R. Sharpe, Kerstin W oltje,
Katharina T. Wei , Markus Albert, Uwe Seidl, Josef Schr oder,
Christian Morsczeck, Lukas Prantl, Claus Duschl,
Stine Falsig Pedersen, Martin Gosau, Mark Berneburg,
Otto S. Wolfbeis, Michael Landthaler, Philipp Babilas

Contents

1. Supplementary Figures (pp. 2-11)

- Figure S1: Cross-sensitivity of pO₂/pH-signals and temperature sensitivity
- Figure S2: pH-stability of pH-adjusted media
- Figure S3: WST-1 tests of keratinocytes cultured in pH-adjusted media
- Figure S4: Stability of pH_e-gradients in microfluidic channels
- Figure S5: Cell trajectory lines of all performed keratinocyte migration assays
- Figure S6: Accumulated distance and endpoint y results of microfluidic migration assays
- Figure S7: Cytokine and chemokine secretion patterns of keratinocytes under varying pH_e
- Figure S8: Expression and localization of pH_e-regulatory NHE1 in chronic wounds
- Figure S9: Expression of proton transporters ATP6V1B2 and MCT1 in intact skin and chronic wounds
- Figure S10: NHE1-generated pH_e-gradients in chronic wounds and their impact on epidermal barrier repair

2. Supplementary Tables (pp. 12-14)

- Table S1: Characteristics of patients with chronic venous wounds for imaging
- Table S2: Characteristics of patients with chronic venous wounds for biopsies

3. Supplementary Still Images for Movies (pp. 15-17)

- Still Image for Movie S1: Time-lapse microscopy image sequences of microfluidic keratinocyte migration assay 1
- Still Image for Movie S2: Time-lapse microscopy image sequences of microfluidic keratinocyte migration assay 2
- Still Image for Movie S3: Time-lapse microscopy image sequences of microfluidic keratinocyte migration assay 3

4. Supplementary Macro Legend (p. 18)

1. SUPPLEMENTARY FIGURES

Figure S1

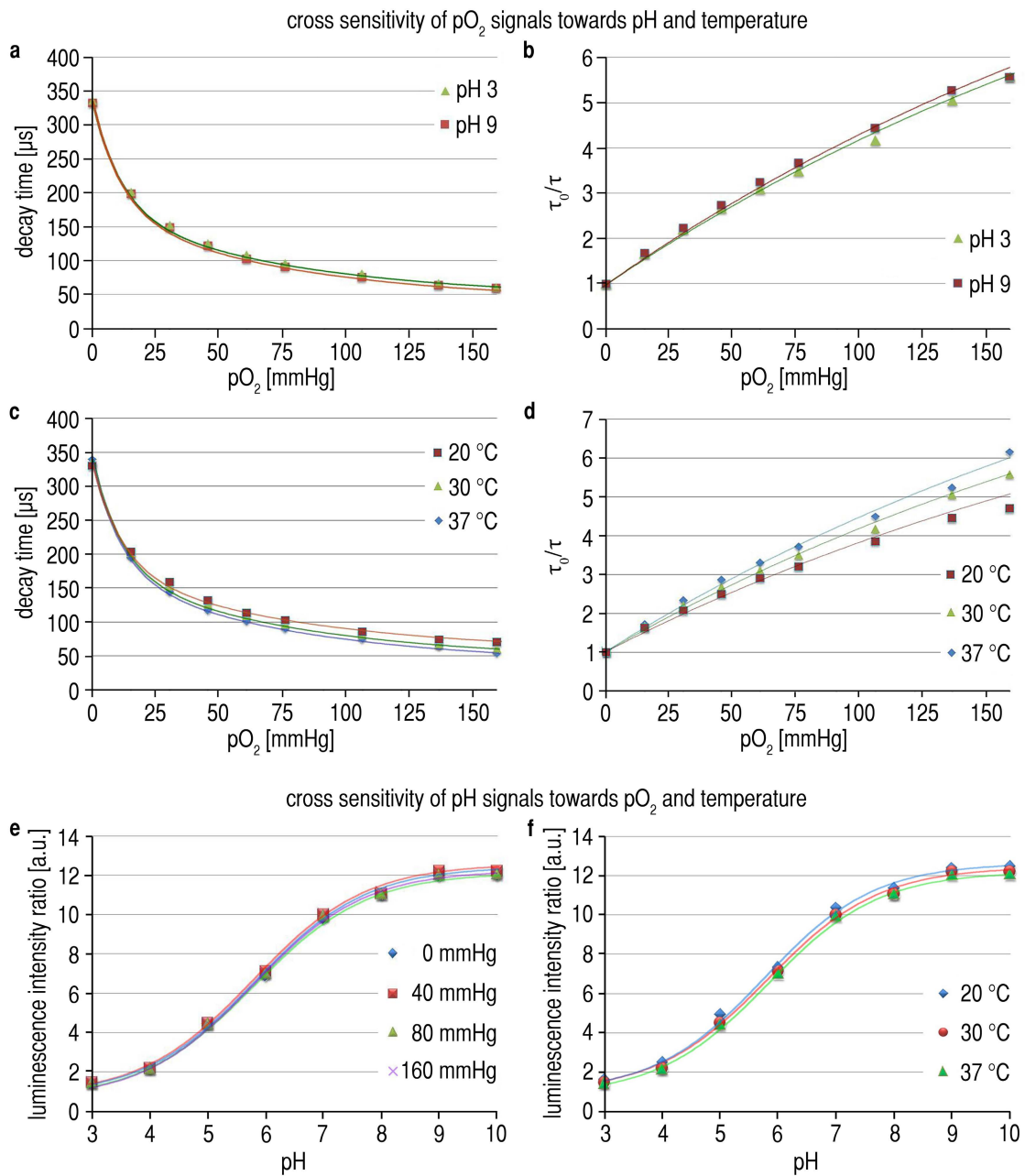


Figure S1: Cross-sensitivity of pO_2 /pH-signals and temperature sensitivity. (A,B) The (A) luminescence decay time and the (B) Stern-Volmer-Plot of luminescence lifetime ratios τ/τ_0 (τ = luminescence lifetime at respective pO_2 , τ_0 = luminescence lifetime at 0 mmHg pO_2) of pO_2 -signals under varying pO_2 are not affected by changes in pH (pH 3 vs. pH 9). (C,D) Temperature, also did not change luminescence decay times or lifetime ratios of pO_2 -signals. (E,F) Luminescence intensity ratios of pH-signals remained unchanged at varying (E) pO_2 and (F) temperatures.

Figure S2

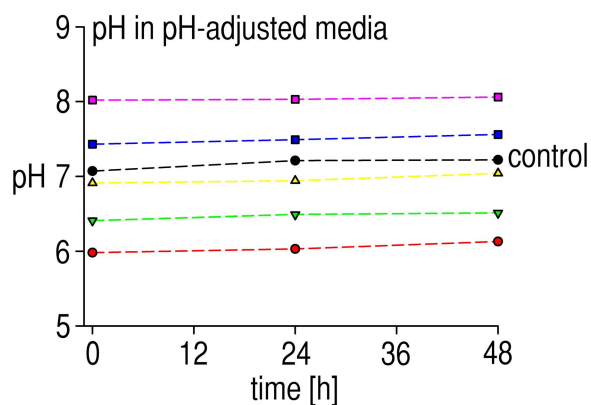


Figure S2: pH-stability of pH-adjusted media. pH was adjusted in culture media to pH 6, 6.5, 7, 7.5, and 8 as outlined in **Materials and Methods**. Stability of pH in pH-adjusted media and of unmodified culture medium was measured with standard pH-electrodes at 0, 24, and 48 h after pH-adjustment. No relevant change of pH in pH-adjusted media was detected over 48 h, the maximum culture time with pH-modified media in all experiments.

Figure S3

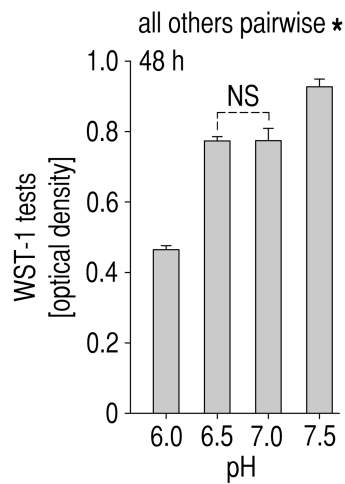


Figure S3: WST-1 tests of keratinocytes cultured in pH-adjusted media. Cell viability increased with rising pH_e , confirming results obtained using ATP-bioluminescence assays (**Fig. 3B**). After 48 h, keratinocyte viability was highest at pH_e of 7.5 and lowest at pH_e of 6.0. $n = 6$, mean \pm s.e.m., NS = not significant, ANOVA $p < 0.001$ and $*p < 0.05$ in post-hoc Holm-Sidak tests.

Figure S4

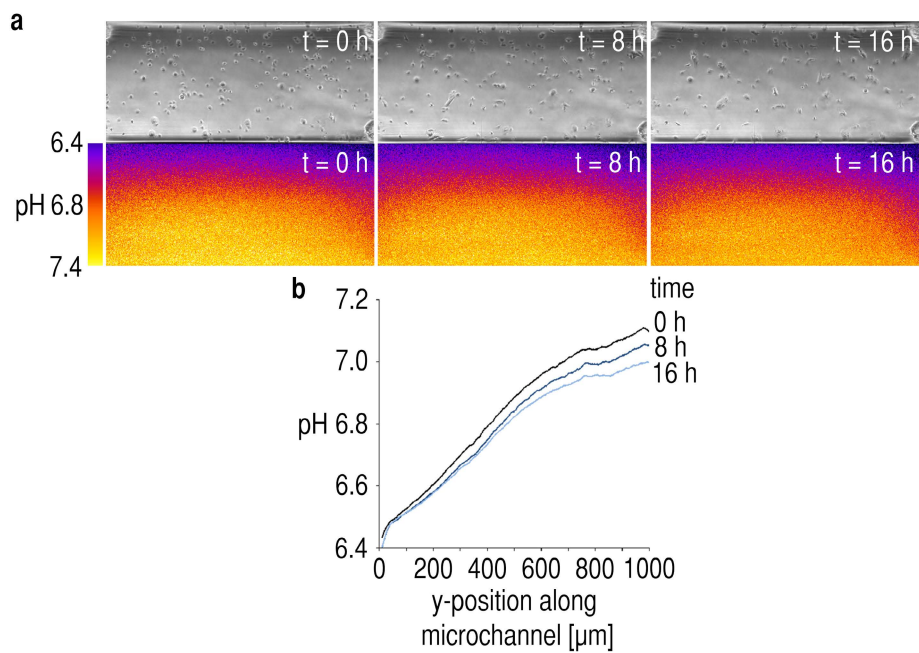


Figure S4: Stability of pH_e-gradients in microfluidic channels. (A) Brightfield and pH-visualization (pseudocolor images) of a representative microfluidic keratinocyte migration assay at different time points throughout the experiment. pH_e-gradients were visualized by ratiometric analysis of BCECF pH-indicator fluorescence in the channel fluid. (B) Mean pH_e-value along the y axis of the microchannel. pH_e-gradients showed a relatively linear shape and were stable throughout the 16 h time course of the experiment.

Figure S5

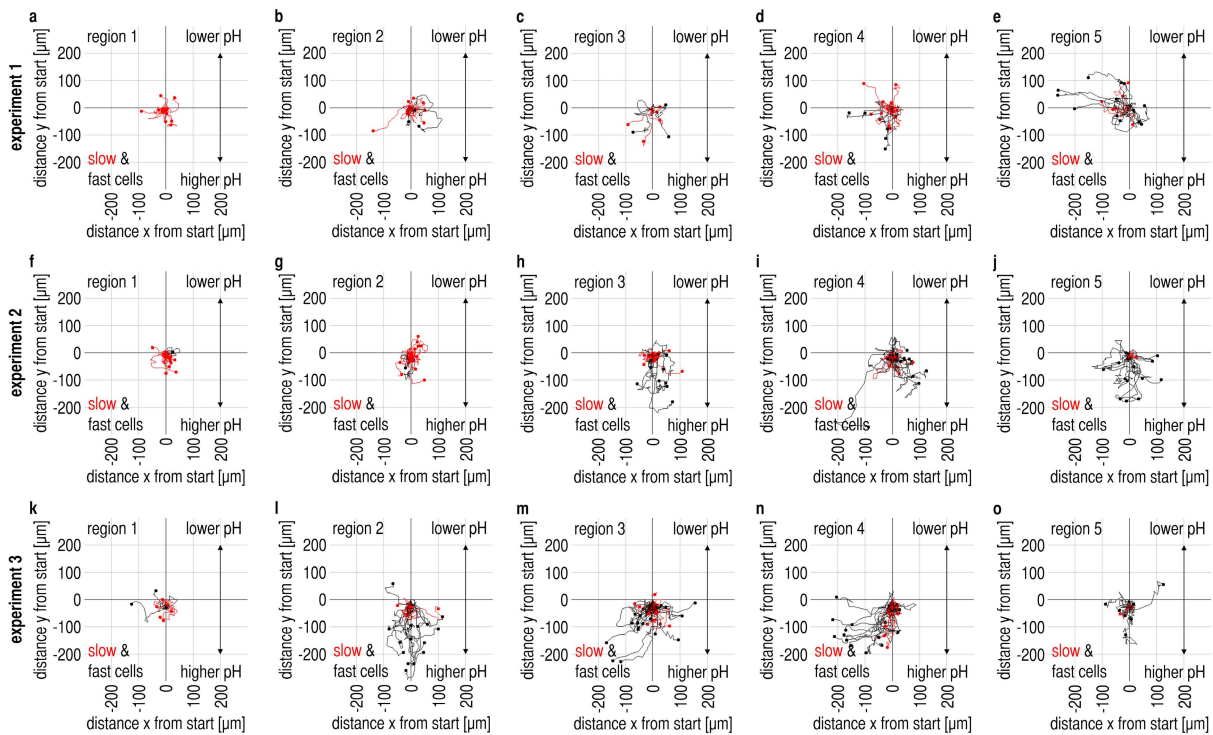


Figure S5: Cell trajectory lines of all performed keratinocyte migration assays. Data of 3 independent experiments (**A-E**, **F-J**, **K-O**) clustered by channel region with increasing mean pH_e from region 1 to region 5 (also see **Movies S1-S3**). Keratinocyte migration was analyzed by time-lapse brightfield microscopy for 16 h. Trajectory lines of the cells were then superimposed (start at $x/y = 0 \mu\text{m}$) with red lines showing slow migrating cells (mean velocity $\leq 12.6 \mu\text{m h}^{-1}$) and black lines showing fast migrating cells (mean velocity $> 12.6 \mu\text{m h}^{-1}$). Throughout the experiments, the proportion of fast cells increased with rising pH_e . Furthermore, migration distance was markedly higher at high pH_e -values when compared to low pH_e -values as found at the wound periphery.

Figure S6

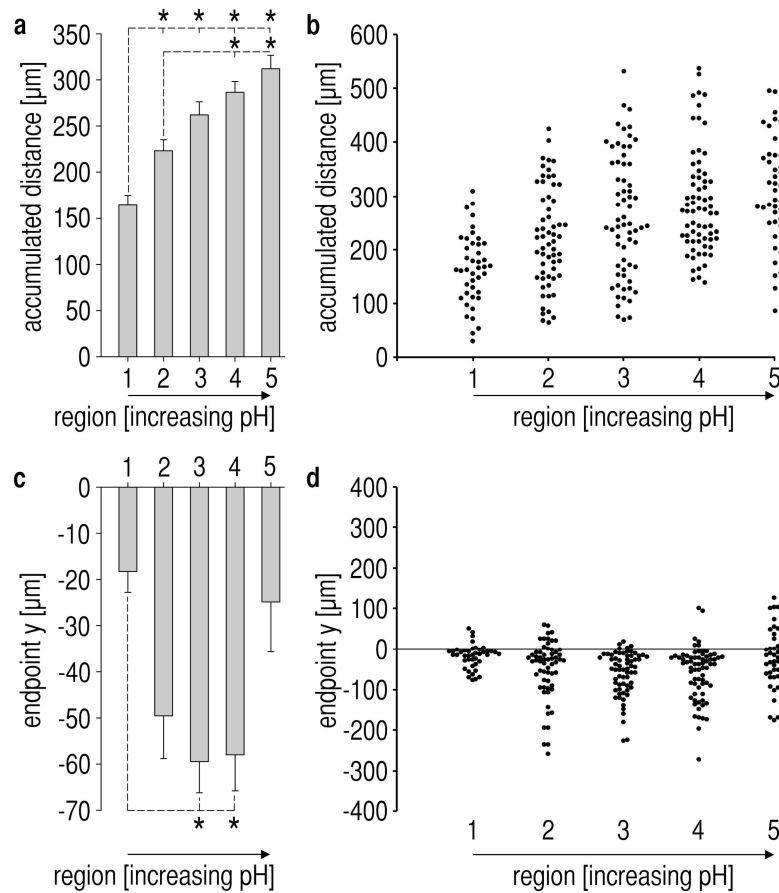


Figure S6: Accumulated distance and endpoint y results of microfluidic migration assays.

(A,B) Mean accumulated distance and respective scatter plot of analyzed single cells (also see **Movies S1-S3**). Accumulated distance increased with higher pH_e and was significantly different between the cells of different channel regions. Mean accumulated distance for cells of region 5 ($\text{pH}_e \sim 7.2$) was almost two times higher than for cells of region 1 ($\text{pH}_e \sim 6.4$). **(C,D)** Endpoint analysis of y-coordinates of cell positions (along the pH_e -gradient) and respective scatter plot of analyzed single cells. The mean endpoint y decreased from $\text{pH}_e \sim 6.4$ to ~ 6.8 (i.e. from region 1 to region 3), and then rose again until $\text{pH}_e \sim 7.2$ (region 5). Thus, keratinocytes at intermediate pH of ~ 6.8 exhibit strongest chemotactic activity towards higher pH_e -values when compared with cells at both higher and lower pH_e . The reason for the reduced chemotactic activity towards higher pH_e -values for cells in low pH_e (~ 6.4) as well as high pH_e (~ 7.2) might be due to a reduced motility or a reduced driving force for directed migration of these cells, respectively. Number of cells tracked in 3 experiments: region 1 ($n = 42$), 2 ($n = 60$), 3 ($n = 65$), 4 ($n = 69$), 5 ($n = 44$). One-way ANOVA on ranks $p < 0.001$, $*p < 0.05$ in post-hoc Dunn's test.

Figure S7

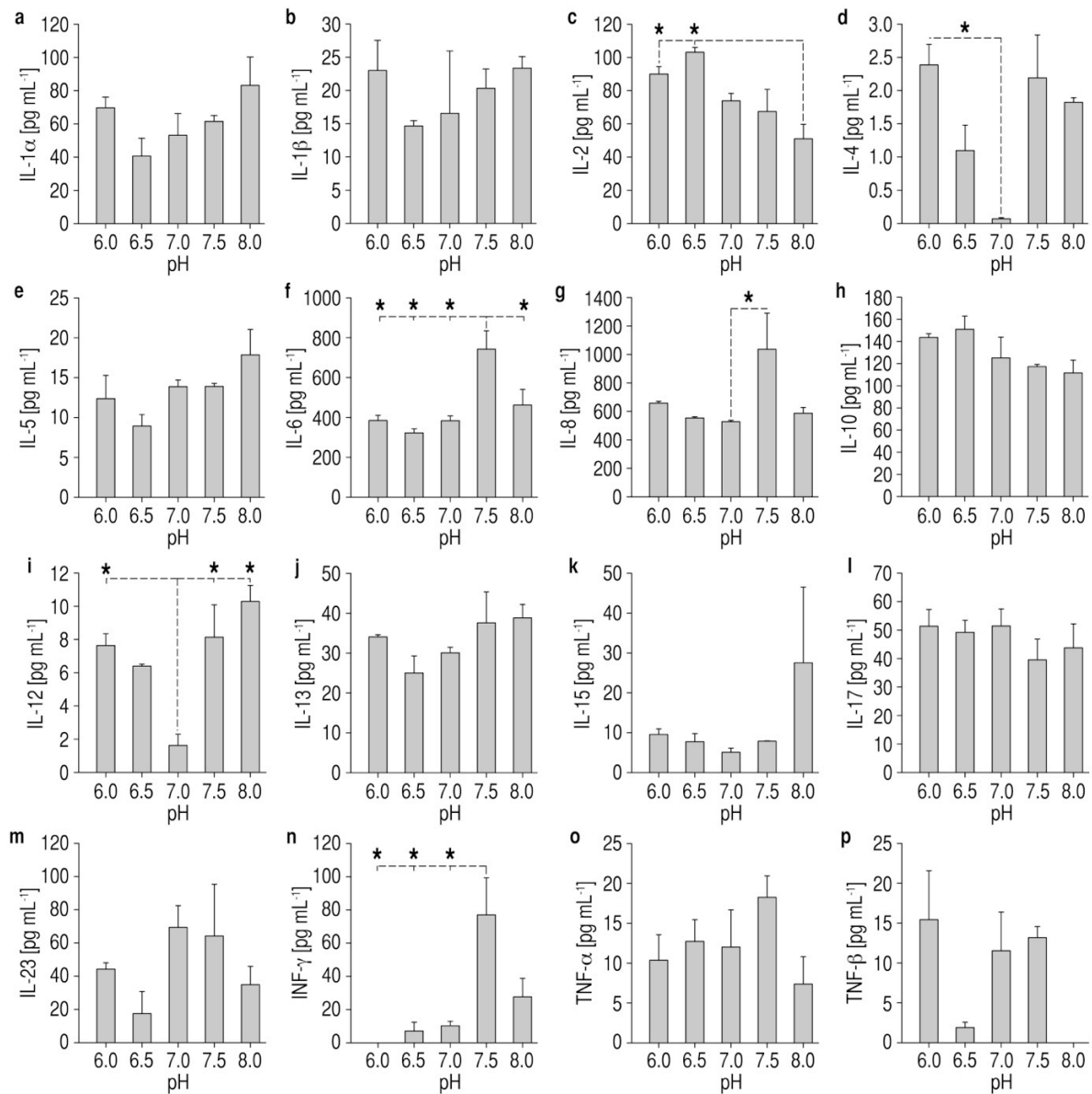


Figure S7: Cytokine and chemokine secretion patterns of keratinocytes under varying pH_e.

We found that **(D,I)** IL-4 and IL-12 were markedly downregulated at pH_e 7.0 when compared to lower or higher pH_e-values. Additionally, keratinocytes cultured at the predominantly high pH_e of 7.5, as found at the wound centers, secreted markedly more **(F,G)** IL-6 and IL-8 (important direct and indirect mediators of keratinocyte proliferation/migration) when compared with those at lower pH_e (as found at the wound periphery). Another interesting finding was that **(N)** interferon- γ (INF γ) release from keratinocytes increased with rising pH_e. INF γ is known to stimulate VEGF production of keratinocytes, and VEGF is a key molecule in neoangiogenesis during healing. At low pH_e, as found at the wound periphery, we found low levels of INF γ in keratinocyte supernatants.

Figure S8

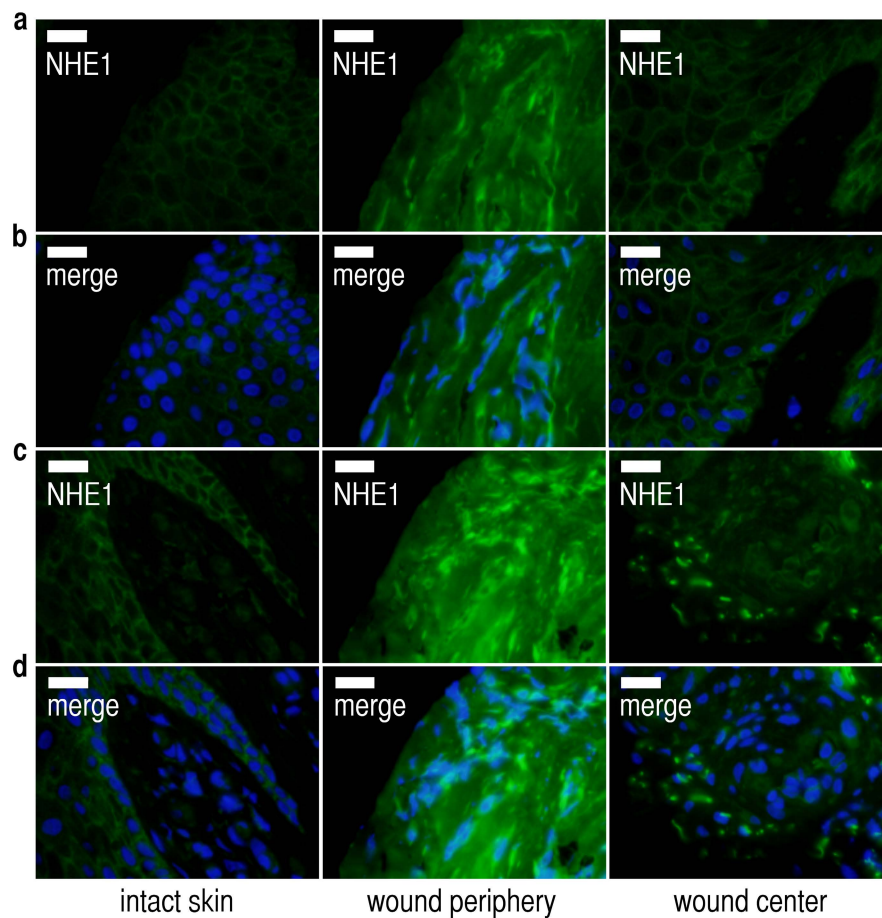


Figure S8: Expression and localization of pH_e -regulatory NHE1 in chronic wounds. (A-D) Additional immunofluorescence images of intact skin, peripheral wound tissue, and central wound tissue from chronic wound patients. Sections were counterstained with (B,D) DAPI (blue) for nuclei staining. Scale bars, 20 μm . (A,C) NHE1 is strongly upregulated in peripheral wound tissue as compared to intact skin and tissue from the wound center.

Figure S9

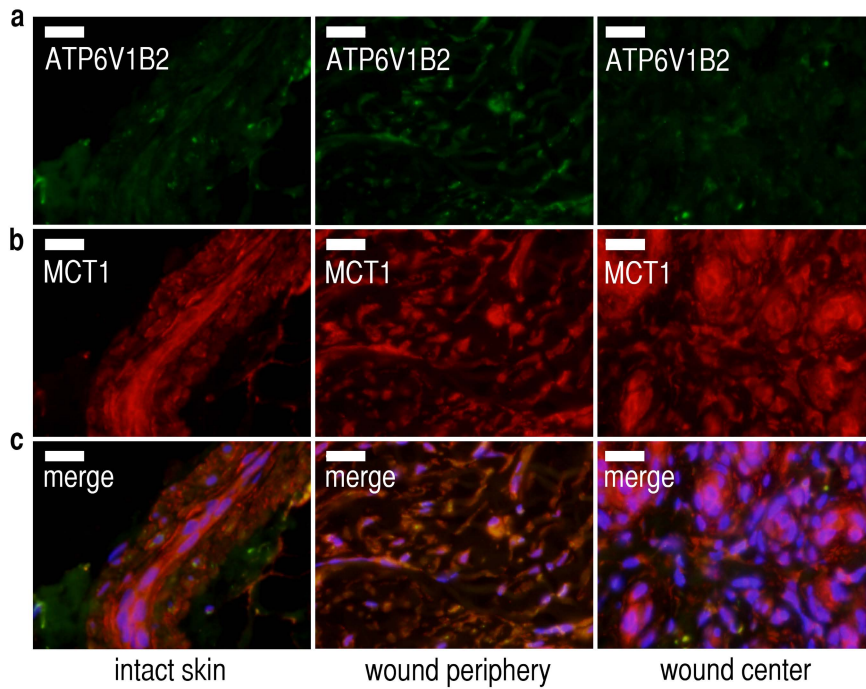


Figure S9: Expression of proton transporters ATP6V1B2 and MCT1 in intact skin and chronic wounds.

(A-C) Additional immunofluorescence images of intact skin, peripheral wound tissue, and central wound tissue from chronic wound patients. Sections were counterstained with **(C)** DAPI (blue) for nuclei staining. Scale bars, 20 μm . $n = 3$. There were virtually no differences in the expression of the **(A)** plasma membrane vacuolar-type ATPases subunit b2 (ATP6V1B2, green) and **(B)** the (H^+ -lactate) monocarboxylate transporter 1 (MCT1, red) between intact skin and wound sections.

Figure S10

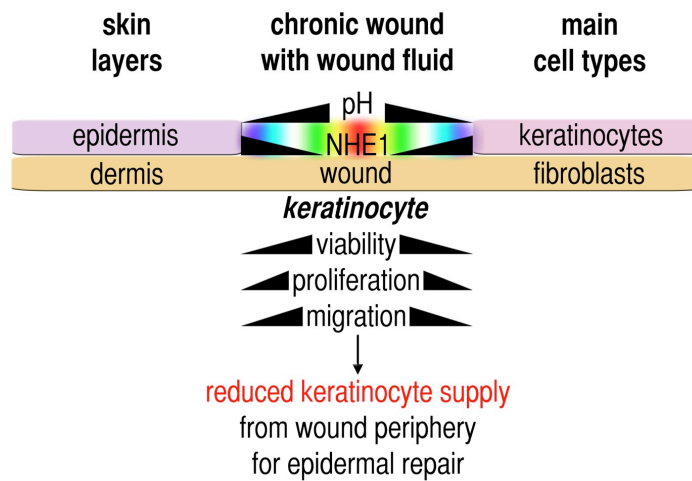


Figure S10: NHE1-generated pH_e-gradients in chronic wounds and their impact on epidermal barrier

repair. We found that pH_e rises with increasing distance from the wound margins. These pH_e-gradients are predominantly generated via centrifugally rising NHE1-expression, a proton transporter crucial for extracellular acidification. The pH_e-gradients found reduce cell viability, proliferation and migration velocity of keratinocytes at the wound periphery. Centripetal keratinocyte recruitment from the wound periphery is critically reduced by the observed pH_e-gradients in chronic wounds, thus disrupting epidermal barrier repair.

2. SUPPLEMENTARY TABLES

Table S1: Characteristics of patients with chronic venous wounds for imaging

No. Sex Age (yrs)	Time of wound persistence (months until imaging)	Localization Size (greatest diameter within wound)	Bacterial colonization (last documented swab, alphabetically)	Main causative disease	Concomitant diseases (as documented in patient history, alphabetically)
1 f 67	14	left medial lower leg 3 cm	enterobacter cloacae pseudomonas aeruginosa staphylococcus aureus	chronic venous insufficiency (CVI)	adipositas permagna arterial hypertension diabetes mellitus type II tinea pedis type IV allergies - amerchol - benzalkonium chloride - cetylstearyl alcohol - formaldehyde - lanolin alcohols
2 m 79	> 60	right lateral lower leg 6 cm	pseudomonas aeruginosa staphylococcus aureus	chronic venous insufficiency (CVI)	arterial hypertension chronic osteomyelitis hypercholesterinemia microangiopathy
3 f 79	48	left medial lower leg 7 cm	not available (12/11 measurement, 08/11 pseudomonas aeruginosa)	chronic venous insufficiency (CVI)	hypothyroidism tinea pedis type IV allergies - amerchol - benzocaine - budesonide - fragrance mix - gentamicin sulfate - nickel - peru balm - phenyl mercury borate xerosis cutis
4 f 73	64	left medial lower leg 4 cm	staphylococcus aureus	chronic venous insufficiency (CVI)	adipositas arterial hypertension hyperkalemia onychomycosis
5 f 73	41	right ventral lower leg 8 cm	corynebacterium spp. proteus mirabilis pseudomonas aeruginosa staphylococcus aureus	chronic venous insufficiency (CVI)	adipositas permagna diabetes mellitus type II diabetic nephropathy erysipelas (of the lower right leg) tinea pedis hypothyroidism
6 f 63	24	right lateral lower leg 7.5 cm	pseudomonas aeruginosa serratia marcescens	chronic venous insufficiency (CVI)	arterial hypertension hypercholesteremia hyperuricemia
7 f 77	14	left lateral lower leg 5 cm	staphylococcus aureus	chronic venous insufficiency (CVI)	adipositas permagna arterial hypertension chronic heart failure chronic renal failure combined aortic vitium diabetes mellitus type II diabetic microrangiopathy diabetic nephropathy diabetic polyneuropathy mitral valve insufficiency postthrombotic syndrome

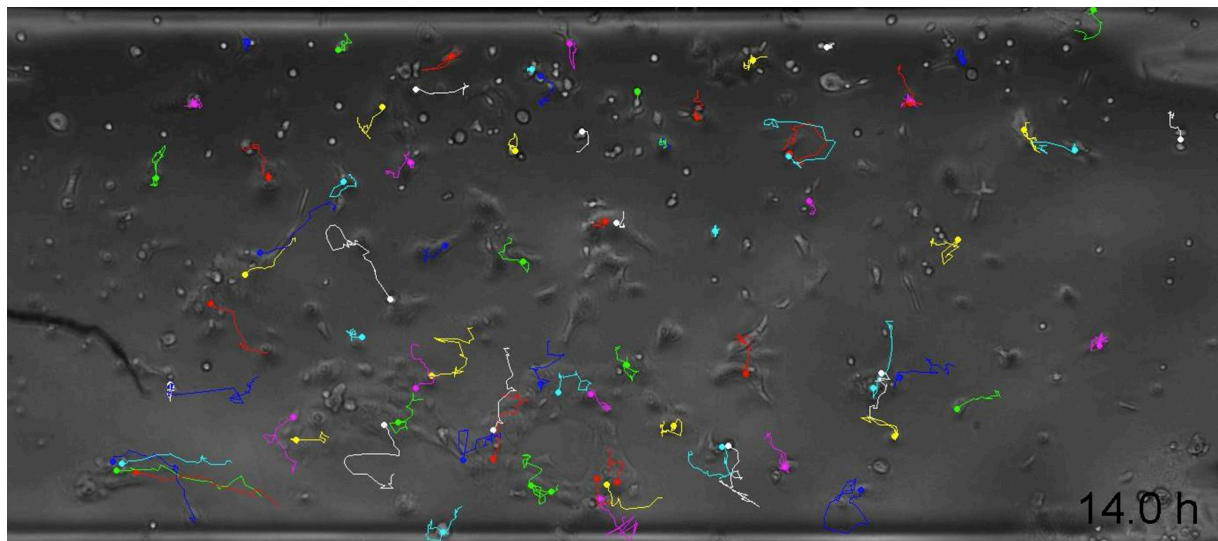
8 m 53	150	left medial lower leg 6 cm	enterobacter cloacae staphylococcus aureus	chronic venous insufficiency (CVI)	diabetes mellitus type II local fasciectomy postthrombotic syndrome resection of saphenous magna vein smoking thrombophlebitis
9 m 51	13	right medial lower leg 4 cm	staphylococcus aureus	chronic venous insufficiency (CVI)	deep leg vein thrombosis (15 years ago)
10 f 66	33	right medial lower leg 3 cm	pseudomonas aeruginosa serratia marcescens	chronic venous insufficiency (CVI)	arterial hypertension chronic heart failure hypercholesteremia onychomycosis percutaneous transluminal coronary angioplasty thyroid subfunction tinea pedis type IV allergies - amerchol - benzoyl peroxide - cetylpyridiniumchloride - cetylstearyl alcohol - cobalt - fragrance mix - framycetin - kanamycin - lanolin alcohols - mercury - neomycin - nickel - nystatin - peru balm - propylene glycole - sodium disulfite - tolu balm - tree moss - turpentine xerosis cutis

Table S2: Characteristics of patients with chronic venous wounds for biopsies

No. Sex Age (yrs)	Time of wound persistence (months until biopsy)	Localization Size (greatest diameter within wound)	Bacterial colonization (last documented swab, alphabetically)	Main causative disease	Concomitant diseases (as documented in patient history, alphabetically)
1 m 65	36	right medial malleolus 5 cm	coagulase-negative staphylococci staphylococcus aureus	chronic venous insufficiency (CVI)	COPD diabetes mellitus type II type IV allergies - amerchol - butyl paraben - benzoyl peroxide - cetylstearyl alcohol - cocamidopropyl betain - diazolidinyl urea - 1,3-diphenylguanidin - dodecyl gallate - ethyl paraben - imidazolidinyl urea - lanolin alcohol - methyl paraben - panthenol - polidocanol - paraben - propylene glycol - propyl paraben - sodium metabisulfite - t-butyl hydrochinone - triethanolamine
2 m 67	27	left medial malleolus 7 cm	proteus mirabilis pseudomonas aeruginosa streptococcus agalactiae	chronic venous insufficiency (CVI)	diabetes mellitus type II diabetic polyneuropathy
3 f 78	60	left medial lower leg 3 cm	pseudomonas aeruginosa staphylococcus aureus	chronic venous insufficiency (CVI)	adipositas arterial hypertension diabetes mellitus type II onychomycosis type IV allergies - amerchol - benzalkonium chloride - cetylstearyl alcohol - fragrance mix - lanolin alcohol - thiram

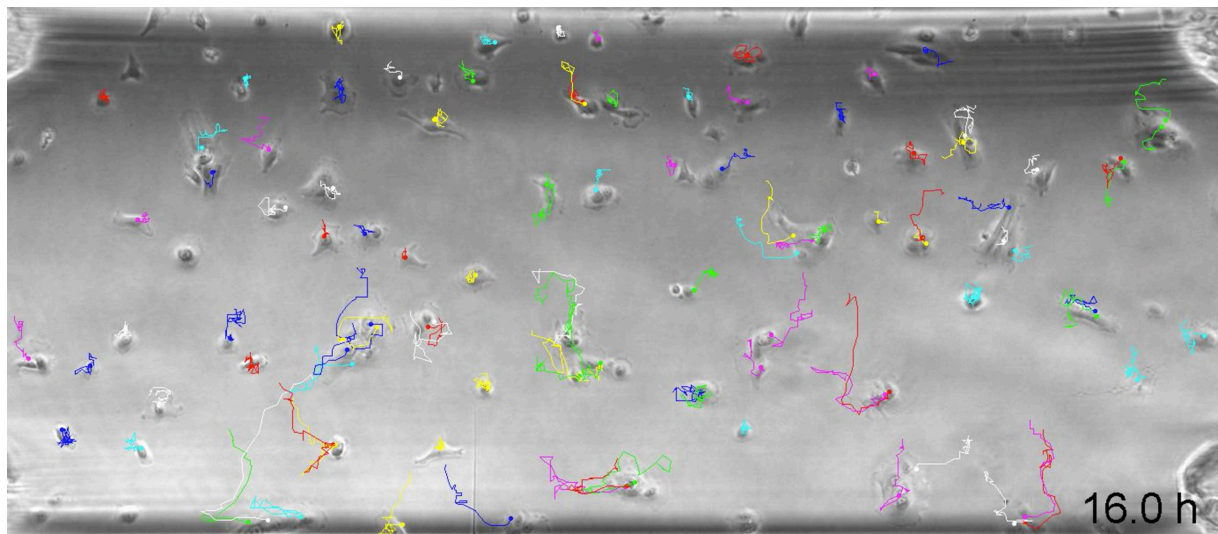
3. SUPPLEMENTARY STILL IMAGES FOR MOVIES

Still Image for Movie S1



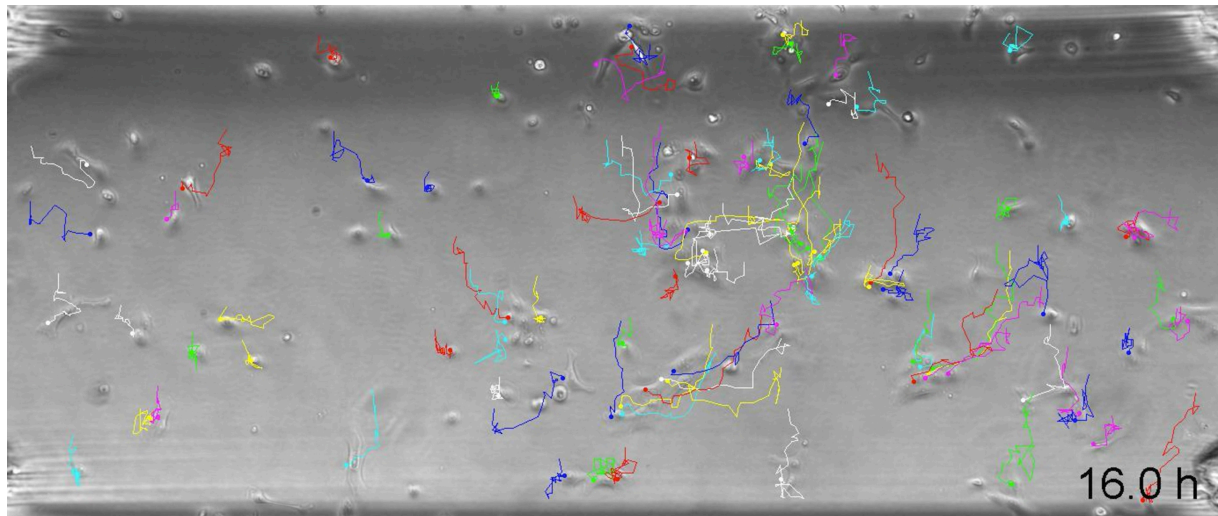
Still Image for Movie S1: Time-lapse microscopy image sequences of microfluidic keratinocyte migration assay 1. Human epidermal keratinocytes were seeded into a fibronectin-coated microfluidic channel and were analyzed for cell migration under no-flow condition while a pH_e -gradient was established in y-direction from $\text{pH} \sim 6.4$ (upper channel boundary) to $\text{pH} \sim 7.2$ (lower channel boundary). Trajectories of the analyzed cells are superimposed on the original images. Frame rate, $\sim 2.5 \text{ frames h}^{-1}$. Throughout all experiments (experiments 1-3 in **Movies S1-S3**), migration velocity rose from low to high pH_e . Accumulated migration distances were highest at high pH_e of ~ 7.2 when compared to pH_e of ~ 6.4 . A detailed analysis of the results is shown in **Fig. 3E-L** and **Figs. S5** and **S6**.

Still Image for Movie S2



Still Image for Movie S2: Time-lapse microscopy image sequences of microfluidic keratinocyte migration assay 2. Human epidermal keratinocytes were seeded into a fibronectin-coated microfluidic channel and were analyzed for cell migration under no-flow condition while a pH_e -gradient was established in y-direction from $\text{pH} \sim 6.4$ (upper channel boundary) to $\text{pH} \sim 7.2$ (lower channel boundary). Trajectories of the analyzed cells are superimposed on the original images. Frame rate, $\sim 2.5 \text{ frames h}^{-1}$. Throughout all experiments (experiments 1-3 in **Movies S1-S3**), migration velocity rose from low to high pH_e . Accumulated migration distances were highest at high pH_e of ~ 7.2 when compared to pH_e of ~ 6.4 . A detailed analysis of the results is shown in **Fig. 3E-L** and **Figs. S5** and **S6**.

Still Image for Movie S3



Still Image for Movie S3: Time-lapse microscopy image sequences of microfluidic keratinocyte migration assay 3. Human epidermal keratinocytes were seeded into a fibronectin-coated microfluidic channel and were analyzed for cell migration under no-flow condition while a pH_e -gradient was established in y-direction from $\text{pH} \sim 6.4$ (upper channel boundary) to $\text{pH} \sim 7.2$ (lower channel boundary). Trajectories of the analyzed cells are superimposed on the original images. Frame rate, $\sim 2.5 \text{ frames h}^{-1}$. Throughout all experiments (experiments 1-3 in **Movies S1-S3**), migration velocity rose from low to high pH_e . Accumulated migration distances were highest at high pH_e of ~ 7.2 when compared to pH_e of ~ 6.4 . A detailed analysis of the results is shown in **Fig. 3E-L** and **Figs. S5** and **S6**.

4. SUPPLEMENTARY MACRO LEGEND

Macro S1: Macro for 2D pO₂/pH_e-calculation. The self-programmed Photoshop macro contains three sub-macros (“macro for preparation”, “macro for slicing”, and “macro for measurement”) that have to be executed following the protocol described in **Materials and Methods**. The first action adapts and standardizes the size of each image and transfers the previously defined wound margins to the raw data TIFF-images. The second action divides raw data from the entire wound into five consecutive regions, starting from the wound periphery towards the center. The final action measures the grayscale mean values of the slices and the entire wound surface and records these values in a CSV-table that can be further used in Excel to convert and calculate respective pO₂/pH_e-data.